Quantum Yields of Hydroxyl Radical and Nitrogen Dioxide from the Photolysis of Nitrate on Ice

Liang Chu and Cort Anastasio*

Atmosphere Science Program, Department of Land, Air, and Water Resources, University of California, One Shields Avenue, Davis, California 95616-8627

Received: April 7, 2003; In Final Form: August 21, 2003

Nitrate photolysis proceeds via two major channels at illumination wavelengths above 290 nm: $NO_3^- + h\nu\ (+H^+) \rightarrow NO_2 + {}^\bullet OH$ (1) and $NO_3^- + h\nu \rightarrow NO_2^- + O(^3P)$ (2). A recent study determined the quantum yield of reaction 1 on ice by measuring NO_2 production, but suggested their values might be lower bounds because of incomplete recoveries of NO_2. We measured the quantum yield of pathway 1 using an alternate approach, i.e., by following the formation of ${}^\bullet OH$. Our quantum yields for ${}^\bullet OH$ (Φ_{OH}) at 263 K were independent of nitrate concentration and illumination wavelength ($\lambda > 300$ nm), but were dependent upon pH. Values of Φ_{OH} decreased from $(3.6 \pm 0.6) \times 10^{-3}$ at pH 7.0 to $(2.1 \pm 0.8) \times 10^{-3}$ at pH 2.0, where the listed pH values are those of the sample solution prior to freezing. Temperature dependence experiments (239−318 K; pH 5.0) showed that values of Φ_{OH} in ice pellets and aqueous solutions were both well described by the same regression line, $\ln(\Phi_{OH}) = \ln(\Phi_1) = -(2400 \pm 480)(1/T) + (3.6 \pm 0.8)$ (where errors represent $\pm 1\sigma$), suggesting that the photolysis of nitrate on ice occurs in a "quasi-liquid layer" rather than in the bulk ice. Our ice quantum yields between 268 and 240 K are 3−9 times higher, respectively, than Φ_1 values determined previously in ice. Applying our quantum yields to past field experiments indicates that nitrate photolysis can account for the flux of NO_x from sunlit snow in the Antarctic and at Summit, Greenland, but that nitrate was only a minor source of the snowpack NO_x measured during the Alert 2000 campaign in the Canadian Arctic. Additional calculations show that the photolysis of nitrate on cirrus clouds in the upper troposphere is a minor source of NO_x that cannot account for the apparent underestimation of the ratio of NO_x/HNO_3 in current numerical models.

1. Introduction

Recent measurements indicate that the photochemically mediated production and release of NO_x is a common occurrence in surface snowpacks. Measurements at Summit (Greenland),[1−3] Alert (Nunavut, Canada),[4,5] and Neumayer (Antarctic)[6,7] all reveal that sunlit polar snowpacks produce NO_x. Significant photochemical production of NO_x has also been found in snow at midlatitudes (Michigan).[8] Since nitrate is a common trace constituent of snow and ice, and NO_3^- photolysis in solution is known to yield NO and NO_2, a number of previous reports have shown or suggested that nitrate photolysis is at least partially responsible for the measured releases of NO_x.[1−10] This photochemistry could be important for a number of reasons:[1,10−12] as a source of NO_x to the snowpack interstitial air and overlying boundary layer, as a source of highly reactive ${}^\bullet OH$ to snow grains, and as a sink for snowpack nitrate. These reactions (and their subsequent effects) will not only alter the chemistry occurring in the snowpack and boundary layer, but could also affect the ice core records of trace species (e.g., NO_3^-, CH_4, and HOOH) that are used to infer the composition of past atmospheres.

Nitrate photolysis in aqueous solution has been extensively studied and proceeds via two main pathways.[13−17] At wavelengths above 290 nm, the major photolysis channel produces NO_2 and ${}^\bullet OH$

$$NO_3^- + h\nu\ (+H^+) \rightarrow NO_2 + {}^\bullet OH \qquad (1)$$

while the minor channel produces nitrite and oxygen atoms

$$NO_3^- + h\nu \rightarrow NO_2^- + O(^3P) \qquad (2)$$

In aqueous solution at 298 K the quantum yields for reactions 1 and 2 are approximately 0.017 and 0.0011,[14,15] respectively, although other values have been reported for each reaction.[16]

In contrast to the solution case, the photochemical behavior of nitrate in ice and snow is relatively poorly understood. Dubowski et al. determined the quantum yield of reaction 1 on ice by measuring the release of NO_2,[18] but suggested that their values might be lower bounds because of incomplete recoveries of this product. This same group has also measured Φ_2, with the more recent value of $(1.5 \pm 0.3) \times 10^{-3}$ at 263 K (ref 19) superseding an earlier value of $(4.8 \pm 1.5) \times 10^{-3}$ (ref 18).

The goal of our study was to measure the quantum yield for reaction 1 in ice by following the formation of ${}^\bullet OH$ to avoid complications with quantitatively collecting photoproduced NO_2. We have determined quantum yields for ${}^\bullet OH$ ($\Phi_{OH} = \Phi_1$) as a function of nitrate concentration and pH in ice pellets. In addition, we have measured the temperature dependence of Φ_{OH} for both ice pellets and aqueous solutions.

2. Experimental Methods

2.1. Materials. Sodium nitrate (certified ACS), hydrogen peroxide, acetonitrile (Optima), sodium borate (certified ACS),

* To whom correspondence should be addressed. Phone: (530) 754-6095. Fax: (530) 752-1552. E-mail: canastasio@ucdavis.edu.

10.1021/jp0349132 CCC: $25.00
Published on Web 10/21/2003

sulfuric acid (Optima), and perchloric acid (Optima) were obtained from Fisher. Benzoic acid (99%), sodium benzoate (99%), and *m*-hydroxybenzoic acid (99%) were obtained from Aldrich, while *p*-hydroxybenzoic acid (98%) was obtained from TCI America. All chemicals were used as received. Purified water ("Milli-Q water") was obtained from a Milli-Q Plus system (≥18.2 MΩ cm).

2.2. Ice Sample Preparation. Ice samples were prepared in a frame consisting of a PVC or Teflon template placed on a quartz backing. The template was a 45 mm × 12 mm × 5 mm piece of material containing a 12 mm × 9 mm × 5 mm hole corresponding to the size and position of the light beam in the illumination system. Samples were prepared by placing the template onto a 45 mm × 12 mm × 1 mm quartz slide and then pipetting 150 μL of Milli-Q water into the well created by the hole in the template. This pure water ice "base" was then frozen by cooling from room temperature to the temperature of the experiment at a rate of −1 K min^{-1} in the ice preparation chamber described below. After the base was frozen, the chamber was kept at the experiment temperature and 50 μL of sample solution was pipetted onto the base and allowed to sit until frozen. This volume of sample solution was small enough that the solution contacted only the pure ice base and did not touch the PVC or Teflon walls of the template. Sample solutions contained known concentrations of $NaNO_3$ and benzoic acid (to trap photoformed •OH; see section 2.3) in Milli-Q water and were adjusted to the desired pH with sulfuric acid (pH 2 to 5) or borate (pH 6 and 7). Note that the terms "benzoic acid" and "BA" here are both used to refer to the sum of benzoic acid and benzoate; stock solutions of 14 mM BA contained 1.3 mM benzoic acid and 12.7 mM sodium benzoate. In addition, all listed concentrations (e.g., BA and NO_3^-) and pH values are for the sample solutions prior to freezing unless specified otherwise.

The ice preparation chamber (100 mm × 100 mm × 50 mm) was a custom-designed unit (Paige Instruments) consisting of a copper block base, Teflon walls, and a removable aluminum top with a glass window. The chamber was cooled by two Peltier units that were attached to the bottom of the copper block base and were run by a custom-designed, programmable, computer-controlled temperature controller. Temperatures in the chamber (239−268 K) were monitored by a thermocouple embedded in the copper block, near its top.

2.3. •OH Measurements. Hydroxyl radicals were characterized by using a chemical probe technique where photoformed •OH reacts with benzoic acid (BA) to form stable, measurable products including *p*-hydroxybenzoic acid (*p*-HBA) and *m*-hydroxybenzoic acid (*m*-HBA):[20,21]

$$\mathrm{BA} + {}^{\bullet}\mathrm{OH} \rightarrow p\text{-HBA} + m\text{-HBA} + \text{other} \qquad (3)$$

We used high concentrations of benzoic acid to trap all of the hydroxyl radicals produced during illumination. To determine the concentration of BA required to scavenge all •OH, we performed two experiments where we measured the rate of *p*-HBA formation as a function of added benzoic acid. The first experiment used a pH 5.0 sample solution (100 μM NO_3^- and 40−1000 μM BA) frozen and illuminated at 263 K; the second test used similar conditions (same pH and temperature) except that $[NO_3^-]$ = 3000 μM and [BA] = 250−6000 μM. In both cases the rate of *p*-HBA formation increased with benzoic acid concentration until $[BA]:[NO_3^-] \geq 1$, above which the rate of *p*-HBA formation was constant. This indicates that all of the •OH radicals were scavenged by BA at $[BA]:[NO_3^-] \geq 1$. All experiments in this study used $[BA]:[NO_3^-]$ ratios of 1.5 or above: for sample solutions with 40−300 μM NO_3^- the BA concentration was 450 μM, while solutions containing 300−3000 μM NO_3^- had 4500 μM benzoic acid.

Ice samples (section 2.2) were illuminated for known time intervals, using 313-nm (or, in a few cases, 334 nm) light from a 1000-W Hg/Xe monochromatic system.[22] Samples were held in a custom-designed (Paige Instruments), Peltier-cooled, temperature-controlled, Teflon-coated copper chamber (38 mm × 26 mm × 70 mm outer dimensions) enclosed in an aluminum housing purged with dry air. In the center of the copper chamber was a 13 mm × 13 mm × 62 mm rectangular opening (with a removable aluminum top) to hold the ice sample, which was placed at the side of the opening nearest the illumination system. A quartz window at this "upstream" side of the opening transmitted light from the illumination system. The light beam (9 mm × 12 mm) from the illumination system passed through the quartz window, into the ice sample, through the quartz slide, and into the back of the sample chamber. The temperature of the sample chamber was monitored with a thermocouple placed into the base of the copper block, just outside the inner sample cavity. Because of the relatively small actinic fluxes in our system (see section 2.4), the low concentrations of nitrate used, and the short pathlengths employed (∼1 mm for the sample solution ice and ∼2 mm for the water ice base), we calculate that illumination would cause negligible heating of the ice sample (<0.3 K over the course of an experiment). Thus the temperature measured in the copper block near the sample cavity should be essentially that of the ice pellet.

At the end of illumination the complete ice sample (frozen sample solution and pure water ice base) was melted in the dark at room temperature in about 5−10 min and then the melted mixture was analyzed for *p*-HBA, using HPLC with UV detection.[20] HPLC conditions were the following: column = Keystone BetaBasic-18 with associated guard column; eluent = 30% CH_3CN and 70% H_2O, mixture adjusted to pH 2 with $HClO_4$; flow rate = 0.60 mL min^{-1}; detection wavelength = 256 nm. Concentrations of *p*-HBA were determined based on calibration standards made in Milli-Q water and run during the day of the illumination experiment.

Initial rates of *p*-HBA formation during illumination ($R^*_{p-\mathrm{HBA},\lambda}$) were determined from plots of [*p*-HBA] versus illumination time by using a linear regression fit or, in a very few cases, an exponential fit, depending on the shape of the data.[20] For each illuminated set of ice samples, rates of *p*-HBA formation were also measured in two controls: (1) in a dark control under identical conditions (sample composition and temperature) except for no illumination (R_{Dark}) and (2) in an illuminated blank control with identical conditions as the sample except that no nitrate was added ($R_{\mathrm{Blank},\lambda}$). The corrected formation rate of *p*-HBA in the illuminated sample was then calculated as

$$R_{p-\mathrm{HBA},\lambda} = R^*_{p-\mathrm{HBA},\lambda} - R_{\mathrm{Dark}} - R_{\mathrm{Blank},\lambda} \qquad (4)$$

As shown in Figure 1, there was generally no formation of *p*-HBA in samples kept in the dark and rates of *p*-HBA formation in the illuminated blanks were typically very small compared to the rates in the corresponding illuminated samples. Corrected rates of *p*-HBA formation were converted to rates of •OH formation ($R_{\mathrm{OH},\lambda}$) by using the yield of *p*-HBA formed from the reaction of •OH with BA ($Y_{p-\mathrm{HBA}}$):[20]

$$R_{\mathrm{OH},\lambda} = R_{\mathrm{p-HBA},\lambda}/Y_{p-\mathrm{HBA}} \qquad (5)$$

Values of $Y_{p-\mathrm{HBA}}$ were measured in illuminated (313 nm) ice samples (section 2.2) made from sample solutions containing

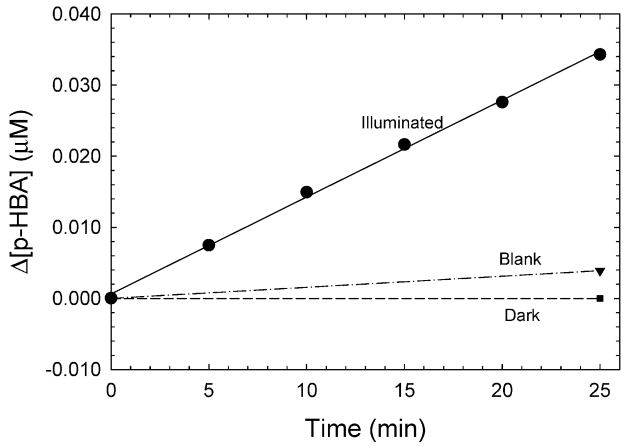

Figure 1. Photoformation of *p*-hydroxybenzoic acid (*p*-HBA) during 313-nm illumination of a frozen (263 K) sample solution composed of 200 μM NO_3^- and 450 μM BA, adjusted to pH 5.0. The solid circles represent data for illuminated frozen samples, while the squares represent *p*-HBA concentrations in an identical frozen sample kept in the dark. The inverted triangles correspond to the formation of *p*-HBA in a blank control (i.e., an illuminated frozen sample solution that contained no nitrate, 450 μM BA, and was adjusted to pH 5.0).

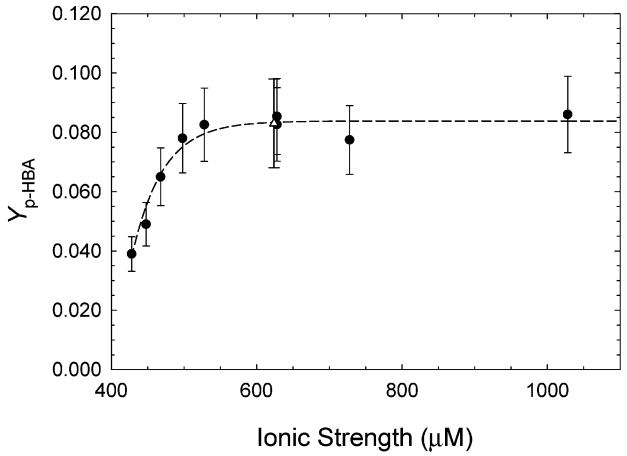

Figure 2. Yield of *p*-HBA formed from the reaction of •OH with benzoic acid ($Y_{p-\mathrm{HBA}}$) as a function of the sample solution ionic strength (pH 5.0) in solutions containing HOOH, BA, and variable amounts of Na_2SO_4. Values of $Y_{p-\mathrm{HBA}}$ were determined by two methods: $R_{p-\mathrm{HBA}}$/calcd R_{OH} (eq 6; solid circles) or $R_{p-\mathrm{HBA}}/R_{\mathrm{BA}}$ (eq 7; open triangle). The dashed line is an exponential fit to all of the experimental data points. One data point (I = 7.1 mM, $Y_{p-\mathrm{HBA}}$ = 0.088; Table S1) is not shown in the figure, but is included in the exponential fit.

HOOH (as a photochemical source of •OH) and benzoic acid and adjusted to a given pH with H_2SO_4. We used two methods to determine $Y_{p-\mathrm{HBA}}$. In the first, we prepared sample solutions with 450 μM BA and 100 μM HOOH and measured the formation of *p*-HBA during illumination. Yields of *p*-HBA from the •OH + BA reaction were determined by using the ratio of the measured (corrected) rate of *p*-HBA formation to the calculated rate of •OH formation from HOOH photolysis ("calcd $R_{\mathrm{OH},\lambda}$"):

$$Y_{p-\mathrm{HBA}} = \frac{R_{p-\mathrm{HBA},\lambda}}{\text{calcd } R_{\mathrm{OH},\lambda}} = \frac{R_{p-\mathrm{HBA},\lambda}}{2.303 I_\lambda \Phi_{\mathrm{HOOH}\rightarrow\mathrm{OH},\lambda} \epsilon_{\mathrm{HOOH},\lambda} [\mathrm{HOOH}] l} \quad (6)$$

where I_λ is the actinic flux in the sample chamber (section 2.4), $\Phi_{\mathrm{HOOH}\rightarrow\mathrm{OH},\lambda}$ is the quantum yield of •OH from HOOH photolysis (extrapolated from the temperature dependence reported in ref 15), $\epsilon_{\mathrm{HOOH},\lambda}$ is the molar absorptivity of HOOH (assumed to be the same as the room-temperature value of 0.37 M^{-1} cm^{-1} at 313 nm; ref 23), [HOOH] is the molar concentration of hydrogen peroxide, and l is the effective path length of the sample (cm). The product $I_\lambda \times l$ in eq 6 was determined by using 2-nitrobenzaldehyde actinometry performed under the same conditions as the $Y_{p-\mathrm{HBA}}$ experiment (see section 2.4). In the second method we employed low concentrations of benzoic acid (10−14 μM) and HOOH (4−6 μM) and measured the rate of formation of *p*-HBA (subsequently corrected for R_{Dark} and $R_{\mathrm{Blank},\lambda}$) and the rate of loss of BA ($R_{\mathrm{BA},\lambda}$) simultaneously in the illuminated samples. Yields of *p*-HBA were then determined as

$$Y_{p-\mathrm{HBA}} = R_{p-\mathrm{HBA},\lambda}/R_{\mathrm{BA},\lambda} \quad (7)$$

Note that this assumes that all BA loss was a result of •OH formed from HOOH photolysis, which should be the case in our experiments.

To ensure that $Y_{p-\mathrm{HBA}}$ values could be applied to our nitrate photolysis experiments, we determined *p*-HBA yields under the same range of conditions used in the nitrate experiments. As shown in Figure 2, $Y_{p-\mathrm{HBA}}$ varied nonlinearly with the ionic strength (I) of the sample solution (pH 5.0, 263 K), increasing from 0.039 at I = 428 μM to 0.084 at I > 600 μM. This relationship is well described by the equation $Y_{p-\mathrm{HBA}} = -1172.5550 + 1172.6388(1 - \exp(-0.0237 \times I))$ ($R^2 = 0.962$), where the ionic strength is the sample solution value in μM. To examine the dependence of $Y_{p-\mathrm{HBA}}$ on pH we used ice (263 K) prepared from sample solutions of pH 2.0−7.0 and with 67 μM added Na_2SO_4 to replace the ionic strength contribution from the 200 μM $NaNO_3$ used for our pH experiments. These measurements revealed that $Y_{p-\mathrm{HBA}}$ has a relatively weak pH dependence, increasing from 0.058 ± 0.016 at pH 2.0 to 0.084 ± 0.014 at pH 7.0, and follows the formula $Y_{p-\mathrm{HBA}} = -0.0011(\mathrm{pH})^2 + 0.0154(\mathrm{pH}) + 0.0318$ ($R^2 = 0.978$; data in Table S1 of Supporting Information). In contrast to the pH 5.0 case, at 263 K in ice prepared from sample solutions of pH 2.0 there was no ionic strength dependence; the average value of $Y_{p-\mathrm{HBA}}$ in these experiments (0.063 ± 0.014) was consistent with that from the pH-dependence experiment. Finally, we examined the temperature dependence of $Y_{p-\mathrm{HBA}}$ (pH 5.0 sample solution with 67 μM added Na_2SO_4) and found that there was no significant difference over the range of 243−268 K, with an average value of 0.081 ± 0.014, consistent with the result from Figure 2. Values of $Y_{p-\mathrm{HBA}}$ are tabulated in the Supporting Information (Table S1).

2.4. Calculation of •OH Quantum Yield. On the day of each experiment the surface-area normalized actinic flux ($I_\lambda l$) in the sample chamber was measured by using ice pellets of the same size and composition as the nitrate-containing samples except for the addition of 4 μM 2-nitrobenzaldehyde (2NB) as a chemical actinometer. For the low light-absorbing conditions of our actinometry, the measured rate constant for 2NB loss ($j_{2\mathrm{NB},\lambda}$) is related to actinic flux through[24]

$$j_{2\mathrm{NB},\lambda} = 2.303 I_\lambda \epsilon_{2\mathrm{NB},\lambda} \Phi_{2\mathrm{NB},\lambda} l \quad (8)$$

where $\epsilon_{2\mathrm{NB},\lambda}\Phi_{2\mathrm{NB},\lambda}$ is the product of the molar absorptivity and quantum efficiency of 2NB (640 M^{-1} cm^{-1} at 313 nm and 300 M^{-1} cm^{-1} at 334 nm, both at 293 K; ref 24) and l is the effective path length of the sample (cm). Actinometry performed on ice pellets with and without the chemical components used for the •OH measurements (i.e., $NaNO_3$, BA, and H_2SO_4) showed that the presence of these chemicals had no effect on

measured values of $j_{2NB,\lambda}$. We also found that $j_{2NB,\lambda}$ was independent of temperature in the range 243−268 K, suggesting that room-temperature values for the product $\epsilon_{2NB,\lambda}\Phi_{2NB,\lambda}$ can be used at lower temperatures. The average value of $j_{2NB,313}$ in our experiments was 0.266 s^{-1}, corresponding to a surface-area normalized actinic flux of 2.5×10^{17} photons cm^{-2} s^{-1} (160 mW cm^{-2}). As mentioned above, only a small fraction (∼0.1%) of this incident light was absorbed by the nitrate-containing ice pellets in our experiments.

Under these low light-absorbing conditions the rate of •OH formation can be expressed as

$$R_{OH,\lambda} = 2.303\, I_\lambda \epsilon_{NO_3^-,\lambda} \Phi_{OH,\lambda} l [NO_3^-] \quad (9)$$

where $\epsilon_{NO_3^-,\lambda}$ is the molar absorptivity of nitrate (5.3 M^{-1} cm^{-1} at 313 nm; see section 2.5), $\Phi_{OH,\lambda}$ is the quantum yield of •OH from nitrate photolysis, and $[NO_3^-]$ is the molar concentration of nitrate. Rearranging eq 8 to solve for I_λ and substituting that into eq 9 produces an expression for the quantum yield of •OH

$$\Phi_{OH,\lambda} = \frac{\epsilon_{2NB,\lambda}\Phi_{2NB,\lambda}R_{OH,\lambda}}{j_{2NB,\lambda}\epsilon_{NO_3^-,\lambda}[NO_3^-]} \quad (10)$$

Note that values of $R_{OH,\lambda}$ might include small contributions from the photolysis of nitrite and nitrous acid, which are formed during nitrate photolysis (reaction 2). However, a kinetic model of the nitrate, nitrite, and nitrous acid reactions in our system indicates that <8% and <14% of our experimentally measured •OH was from nitrite and nitrous acid in ice from sample solutions of pH 5.0 and 2.0, respectively. Because these upper bound contributions are smaller than our experimental uncertainties (the average relative standard deviation in our ice experiments was 20%), we did not adjust our nitrate $\Phi_{OH,\lambda}$ values for possible contributions from NO_2^- and HNO_2 photolysis. Finally, because values of $\Phi_{OH,\lambda}$ are independent of illumination wavelength in the 300-nm band (see section 3.3), we use the term "Φ_{OH}" in this paper instead of wavelength-specific nomenclature such as $\Phi_{OH,313}$.

2.5. Molar Absorptivities of Nitrate as a Function of Temperature. While the 200-nm absorption band of nitrate on ice has been measured,[25] there are no published ice measurements for the weaker 300-nm band. Because the weak absorption in this latter band makes it difficult to measure molar absorptivities on ice, we instead used values extrapolated from the temperature dependence of absorbance in aqueous solution. Absorbance spectra of four aqueous nitrate solutions (27−108 mM) and a Milli-Q blank were measured in a Shimadzu UV-2501PC spectrophotometer using a stirred 1.0-cm quartz cell and Milli-Q as reference. The sample cell holder was cooled (276−298 K) with chilled water from a recirculating water bath. The molar absorptivity at each wavelength (250−360 nm) was determined as the slope of the linear regression fit to the data of absorbance versus nitrate concentration.

As shown in Figure 3, $\epsilon_{NO_3^-,\lambda}$ changes very little across the temperature range examined. In particular, the molar absorptivity of nitrate at 313 nm exhibited no significant dependence on temperature, with an average value of 5.31 ± 0.03 M^{-1} cm^{-1} between 276 and 298 K. The best fit values of the molar absorptivities at all temperatures and wavelengths are listed in the Supporting Information (Table S2).

2.6. Measurements of Φ_{OH} in Aqueous Solution. Aqueous solutions contained 200 μM $NaNO_3$ and 450 μM benzoic acid, and were adjusted to pH 5.0 with sulfuric acid. Samples were illuminated with 313-nm light in stirred 1-cm cells; small aliquots were removed at measured time intervals and analyzed for *p*-HBA. Rates of •OH formation were determined with use of eq 5, using a newly determined value for Y_{p-HBA} (0.19 ± 0.01) that is consistent with that reported previously.[20] The quantum yield of •OH was calculated by using eq 10, where $j_{2NB,\lambda}$ was the value measured in aqueous 2NB (4 μM) on the same day as the nitrate photolysis experiment.

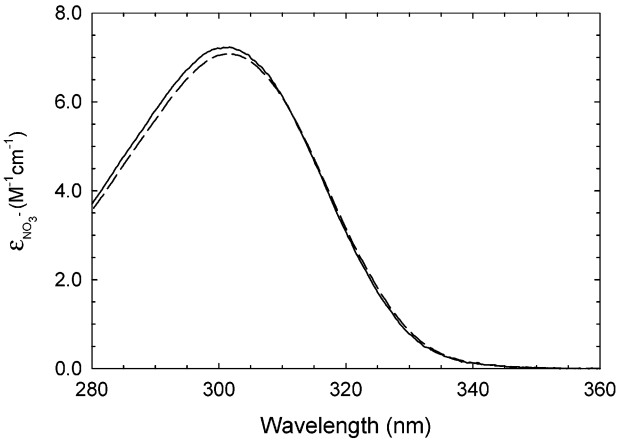

Figure 3. Base-10 molar absorptivities of aqueous nitrate at 278 K (solid line) and 293 K (dashed line). Values of $\epsilon_{NO_3^-,\lambda}$ as a function of temperature and wavelength are tabulated in the Supporting Information (Table S2).

2.7. Estimation of Nitrate Concentration and pH in the Quasi-liquid Layer. Slow freezing of an aqueous solution segregates the components into frozen pure water ice and a disordered, possibly heterogeneous, "quasi-liquid" layer (QLL) containing the solutes.[26−29] This interfacial QLL has not been well characterized and its properties often seem to depend on the analytical method employed to study it.[26−29] As described below, we estimated the nitrate concentration and pH in the QLL for our experiments using the freezing-point depression due to solutes and the acid-dissociation equilibria for sulfuric, nitric, and benzoic acids. Although the quasi-liquid layer is structurally different from liquid water at the temperatures used here,[26,29] Cho et al.[28] found that, at temperatures above the NaCl eutectic point of 252 K, the measured liquid water fraction in a frozen NaCl solution was similar to that calculated by freezing point depression. Based on this, we have estimated the molality of total solute (m, mol kg^{-1}) in the QLL in our experiments from[30]

$$m = \Delta T/1.86 \quad (11)$$

ΔT here is the freezing point depression, i.e., 273 K − T_{exp}, where T_{exp} is the ice temperature during the experiment (K). Because we froze our sample solutions slowly, we assume that all solutes are excluded from the bulk ice and are present in a (homogeneous) QLL; based on results from the Aerosol Inorganics Model,[31] there should be no formation of nitrate hydrates or solids in our ice pellets. The resulting rough estimates of QLL composition under typical experimental conditions are listed in Table 1.

3. Results and Discussion

3.1. Quantum Yield of •OH in Ice as a Function of Nitrate Concentration. Quantum yields of •OH (Φ_{OH}) from nitrate photolysis in ice were measured at 263 K in frozen sample solutions with different nitrate concentrations at pH 2.0 and 5.0. As shown in Figure 4, Φ_{OH} in the frozen pH 5.0 sample

TABLE 1: Typical Sample Solution Conditions and the Corresponding Estimated Quasi-liquid Layer (QLL) Composition for Ice Pellets at 263 K

sample solution values				ice quasi-liquid layer composition[a]		
pH	[BA] (μM)	[NO_3^-] (μM)	concn factor[c]	ionic strength (M)	[NO_3^-][b] (M)	pH
5.0	450	40	5673	2.6	0.23	4.9
5.0	450	100	5036	2.6	0.50	4.9
5.0	450	200	4241	2.6	0.85	4.9
5.0[d]	450	200	330	5.2	0.066	5.0
5.0	4500	3000	362	2.7	1.1	4.7
2.0	450	150	482	1.4	0.072	−0.36
2.0	4500	3000	216	1.5	0.65	0.17

[a] The total molality in the quasi-liquid layer at 263 K was calculated to be 5.38 mol kg^{-1}, based on the freezing point depression (eq 11) and assuming all solutes were present in the QLL. [b] Total concentration of NO_3^- and HNO_3 in the QLL. [c] Ratio of the total concentration of NO_3^- and HNO_3 in the QLL to the total concentration in the sample solution. [d] Sample solution also contained 5.0 mM added Na_2SO_4 to adjust the ionic strength.

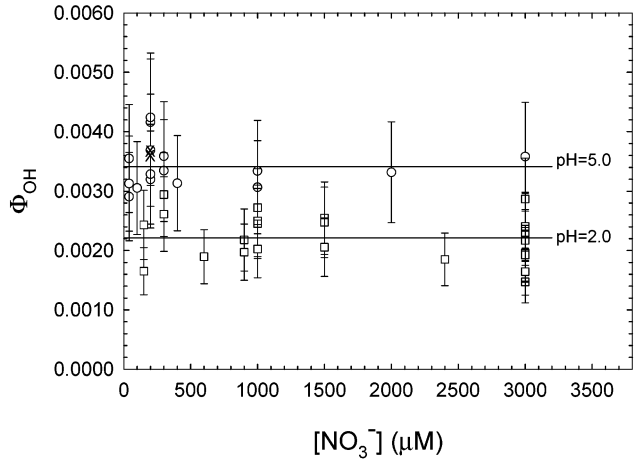

Figure 4. Quantum yields of •OH in ice pellets (263 K; 313-nm illumination) as a function of nitrate concentration in the sample solution. Sample solution composition: pH 5.0 (circles) or 2.0 (squares); [BA] = 450 μM for [NO_3^-] ≤ 450 μM, and [BA] = 4500 μM for [NO_3^-] > 450 μM. Error bars represent $\pm 1\sigma$, calculated based on the uncertainties in $R_{p-HBA,\lambda}$, I_λ, Y_{p-HBA}, $\epsilon_{NO_3^-,\lambda}$, [$NO_3^-$], and the *p*-HBA calibration curve. Horizontal lines indicate the average values for ice made from sample solutions of pH 5.0 ($(3.4 \pm 0.6) \times 10^{-3}$) and 2.0 ($(2.2 \pm 0.5) \times 10^{-3}$). The two "×" points represent pH 5.0 sample solutions that had been adjusted with Na_2SO_4 to the same ionic strength (15 mM) as the corresponding pH 2.0 sample solution.

solutions was independent of the nitrate concentration and had an average value ($\pm 1\sigma$) of $(3.4 \pm 0.6) \times 10^{-3}$. Values of Φ_{OH} in the pH 2.0 sample solutions were also independent of [NO_3^-], but the average value of $(2.2 \pm 0.5) \times 10^{-3}$ was 35% lower than the pH 5.0 average (Figure 4). As described in more detail below, it is unclear why Φ_{OH} is lower in the ice prepared with the pH 2.0 sample solution. To test whether the greater ionic strength in the pH 2.0 solution was responsible, we measured Φ_{OH} in a pH 5.0 sample solution that was adjusted with Na_2SO_4 to the same ionic strength as the pH 2.0 solution. As shown in Figure 4, the addition of Na_2SO_4 had little effect and the average Φ_{OH} in these two experiments, $(3.6 \pm 0.6) \times 10^{-3}$, was identical (within the uncertainties) to the average Φ_{OH} for the other pH 5.0 experiments. This indicates that the ionic strength of the sample solution has no significant effect on Φ_{OH} within the range of ionic strengths tested. Estimated quasi-liquid layer (QLL) concentrations (Table 1) indicate that the pH 2.0 solution and the Na_2SO_4-adjusted pH 5.0 solution had similar nitrate concentrations. However, the quasi-liquid layer pH (QLL

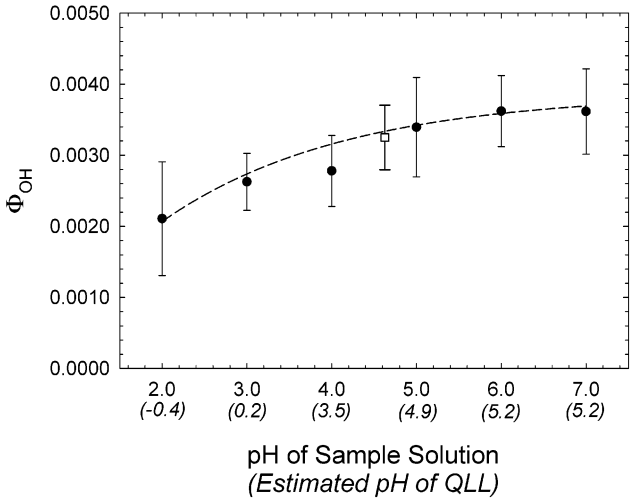

Figure 5. Quantum yields of •OH in ice pellets (263 K, 313-nm illumination) as a function of pH in the unfrozen sample solution. Sample solutions contained 200 μM of either $NaNO_3$ (solid circles) or HNO_3 (open square). The italicized pH values in parentheses are the estimated values in the quasi-liquid layers of the ice pellets; the HNO_3 samples had an estimated QLL pH of 4.5. Each data point represents the average value of 2−24 individual measurements, with error bars of $\pm 1\sigma$. The solid line is an exponential regression fit to the experimental data ($R^2 = 0.961$): $\Phi_{OH} = 0.000587 + 0.00374(1 - \exp(-0.257 \times \text{pH}))$, where the pH is the value in the sample solution.

pH 5.0) resulting from the Na_2SO_4-adjusted pH 5.0 sample was much higher than that resulting from the pH 2.0 solution (QLL pH −0.36), suggesting that differences in pH might be the cause of the observed Φ_{OH} differences.

3.2. Quantum Yield of •OH in Ice as a Function of pH. To explore the pH dependence of Φ_{OH} on ice, we measured values in frozen sample solutions containing 200 μM NO_3^- and with pH values from 2.0 to 7.0, as shown in Figure 5. The estimated pH values in the QLL, which are also listed on the figure, ranged from pH −0.4 (from the pH 2.0 sample solution) to 5.2 (pH 7.0 solution). Φ_{OH} was approximately constant in ice pellets made from sample solutions of pH 5.0 to 7.0, but decreased in ice made from sample solutions with lower pH values. Φ_{OH} in the ice prepared from the pH 2.0 sample solution, $(2.1 \pm 0.8) \times 10^{-3}$, was approximately 40% lower than that obtained for ice made with the pH 7.0 solution, $(3.6 \pm 0.6) \times 10^{-3}$. As shown in Figure 5, the •OH quantum yield in samples prepared with HNO_3 (sample solution pH 4.6) was consistent with the pH trend observed in the other samples, which were prepared with $NaNO_3$.

We examined four possible reasons why Φ_{OH} decreases at lower pH: (1) effects of ionic strength on •OH formation, (2) sensitivity of the yield of *p*-HBA (Y_{p-HBA}) to varying ionic strength or pH, (3) evaporation of HNO_3 from the ice surface, and (4) differences in the behavior of HNO_3 compared to NO_3^-. As discussed in section 3.1, we eliminated the first possible reason since differences in ionic strength had no significant effect on Φ_{OH} under our experimental conditions. We can also eliminate the second possibility since for any given sample experiment we measured Y_{p-HBA} under nearly identical conditions of pH and ionic strength. The third possibility (HNO_3 evaporation at low pH) was ruled out by measuring the concentrations of total nitrate (i.e., HNO_3 and NO_3^-) in ice pellets after being held in the sample chamber in the dark for 20 min, the typical duration of a photochemistry experiment. There was no significant loss (average of <1%) for NO_3^- in ice made from sample solutions with pH values of 2.0 or 5.0.

The final possibility we considered is that the •OH quantum yield and/or molar absorptivity of HNO_3 are lower than those of NO_3^-. This would lead to less •OH production and lower calculated values of Φ_{OH} under more acidic conditions where HNO_3 is more prevalent. However, based on the pK_a for HNO_3 (-1.2 at room temperature[32]), only about 14% of NO_3^- would be converted to HNO_3 under the most acidic conditions of this study (i.e., QLL pH of -0.4 resulting from the pH 2.0 sample solution). Therefore, even if the •OH quantum yield from HNO_3 photolysis was zero, protonation of NO_3^- is unable to explain the ~40% decrease in measured values of Φ_{OH} between the highest and lowest pH values studied (Figure 5). Furthermore, in aqueous solution the estimated values of the •OH quantum yield and molar absorptivity for HNO_3 are not much different from the corresponding values for NO_3^- (ref 33). Thus protonation of NO_3^- to HNO_3 at low pH does not appear to be the reason for the reduction of Φ_{OH} with decreasing pH in the ice pellets. A related possibility is that in the more acidic solutions HNO_3 might be drawn to the air−QLL interface and that this reduces apparent reactivity, perhaps because of separation of HNO_3 from the benzoic acid probe, although we have no mechanism to suggest why this would occur. This surface enhancement of HNO_3 has been observed in very acidic ternary $HNO_3-H_2SO_4-H_2O$ solutions (e.g., 25% HNO_3 and 25% H_2SO_4),[34] but it is unclear whether a similar phenomenon occurs under our milder experimental conditions. Furthermore, unless the pK_a of HNO_3 is higher at the air−QLL interface at these low temperatures (compared to the value in bulk solution at 298 K), the fraction of HNO_3 should be too small (~14%) to produce the pH effect we have measured, as discussed above. Thus at this point we are unable to explain the pH dependence of the •OH quantum yield. However, regardless of the mechanism responsible for the pH dependence of Φ_{OH}, values determined from sample solutions of pH ≥5 should be applicable for many field studies given that melted, bulk snow typically has a pH value of 5 or greater (e.g., ref 35). It should be noted, however, that there are conditions under which the pH of the "disordered" layer on ice or snow surfaces can be significantly lower (e.g., ref 28).

3.3. Wavelength Dependence of Φ_{OH}. To test whether the •OH quantum yield is wavelength dependent, we also measured Φ_{OH} during illumination with 334-nm radiation. Because of the lower molar absorptivity of nitrate at 334 nm (0.34 M^{-1} cm^{-1} at 263 K, interpolated from values in Table S2), we used ice pellets made from sample solutions containing a relatively high nitrate concentration (10 mM) along with 10 mM BA and with a pH of 5.0. The resulting average value of $\Phi_{OH,334}$ at 263 K was $(3.5 \pm 0.5) \times 10^{-3}$ ($N = 3$ determinations), which is statistically indistinguishable from the average value ($(3.4 \pm 0.6) \times 10^{-3}$) obtained with 313-nm illumination of the frozen pH 5.0 sample solutions at 263 K. This suggests that the quantum yield of •OH is independent of illumination wavelength within the 300-nm absorbance band, as found previously for nitrate photolysis in aqueous solution.[15]

3.4. Quantum Yields of •OH in Aqueous Solutions and in Ice Pellets as a Function of Temperature. We measured values of Φ_{OH} in aqueous sample solutions (200 μM $NaNO_3$, 450 μM BA, pH 5.0) between 278 and 318 K. As shown in Figure 5, our •OH quantum yields in solution are very similar to previously reported values, and range from $\Phi_{OH} = (7.2 \pm 1.6) \times 10^{-3}$ at 278 K to $(2.2 \pm 0.5) \times 10^{-2}$ at 318 K. We also measured quantum yields for •OH in ice pellets ($T = 239-268$ K) prepared from sample solutions identical with those described above. As shown in Figure 6, our values of Φ_{OH} in ice ranged from $(1.7 \pm 0.3) \times 10^{-3}$ at 239 K to $(5.4 \pm 1.0) \times 10^{-3}$ at 268 K and were significantly higher than previously reported values.[18]

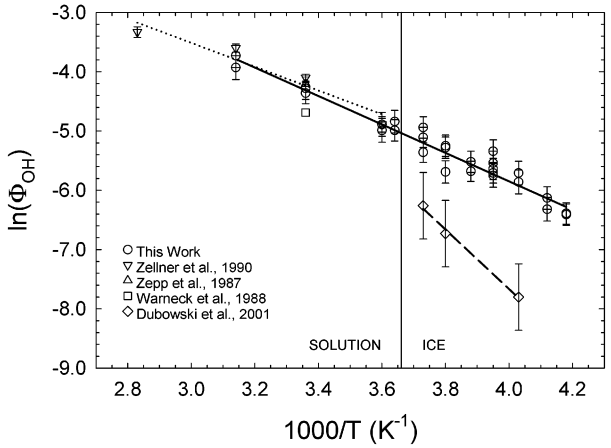

Figure 6. Temperature dependence ($T = 239-318$ K) of Φ_{OH} in aqueous and frozen sample solutions containing 200 μM NO_3^-, 450 μM BA, and adjusted to pH 5.0. The circles are measured data from the present study in both aqueous solution and ice pellets, with errors of $\pm 1\sigma$. The solid line is a linear regression fit to the average value of Φ_{OH} at each temperature for both our solution and ice data (eq 12). The triangles, inverted triangles (with dotted regression line), and squares are solution data from Zepp et al.,[13] Zellner et al.,[15] and Warneck et al.,[14] respectively. The diamonds are measured data of Dubowski et al.[18] in ice pellets. Error bars for these previous sets of data are the unspecified uncertainties reported by the authors.

TABLE 2: Values of E_a and ΔS ($\pm 1\sigma$) for the Formation of •OH and NO_2 from Nitrate Photolysis in Ice and Aqueous Solution[a]

	E_a (kJ mol^{-1})	ΔS (J mol^{-1} K^{-1})
solution values		
this study	19 ± 4	29 ± 6
Zellner et al. (1990)[b]	16 ± 4	19 ± 5
ice values		
this study	20 ± 4	33 ± 7
Dubowski et al. (2001)[c]	42 ± 6	103 ± 22
combined values		
this study	20 ± 4	31 ± 7

[a] The activation energy (E_a) and change in entropy (ΔS) were calculated based on the linear regression fits to the $\ln(\Phi_{OH})$ versus $1/T$ data (Figure 6): $E_a = -\text{slope} \times R \times 10^{-3}$ kJ J^{-1} and $\Delta S = y\text{-intercept} \times R$, where R is the gas constant (8.314 J mol^{-1} K^{-1}). [b] Values calculated based on the pH 4−9 data of Zellner et al.[15] [c] Values calculated based on Figure 5 of Dubowski et al.[18]

It is clear from Figure 6 that our aqueous solution and ice pellet results have essentially the same temperature dependence. This is confirmed by a comparison of the calculated activation energies (E_a) and entropy changes (ΔS) (Table 2): values of E_a and ΔS were statistically indistinguishable between our solution and ice results. Since the same temperature dependence applies to both the ice and aqueous data, we combined all of our Φ_{OH} measurements to obtain a "universal" relationship for the quantum yield of reaction 1:

$$\ln(\Phi_1) = \ln(\Phi_{OH}) = -(2400 \pm 480)(1/T) + (3.6 \pm 0.8) \quad (12)$$

where T is in units of Kelvin, errors represent $\pm 1\sigma$, and the R^2 value is 0.982. At 268 and 240 K, values of Φ_1 determined from eq 12 are 21% and 34% lower, respectively, than corresponding values determined by extrapolating the temperature dependence of the aqueous solution data of Zellner et al.[15]

In contrast, values of Φ_1 from eq 12 are 3 and 9 times higher at 268 and 240 K, respectively, than values obtained from the temperature dependence of the ice data of Dubowski et al.[18]

The fact that our ice pellet and aqueous solution data have the same temperature dependence suggests that the photolysis of nitrate on ice between 239 and 268 K occurs in a quasi-liquid, or disordered, layer rather than in the bulk ice. If NO_3^- photolysis occurred in the bulk ice we would expect the temperature dependence of the ice experiments to differ from the solution experiments in two ways: (1) there would be a noticeable drop in Φ_{OH} (i.e., a discontinuity in Figure 6) when going from solution to ice, and (2) the slope of the ice data would be steeper (more negative) than that of the solution data. These effects are expected because measurement of $^{\bullet}OH$ from nitrate photolysis requires that the initial photoproducts (NO_2 and $^{\bullet}O^-$) diffuse out of the solvent "cage" and away from each other to avoid recombination (e.g., refs 15 and 36 and references therein). Because nitrate diffusion is orders of magnitude slower in ice compared to that in aqueous solution,[37,38] recombination of the initial photoproducts should be more efficient in a bulk ice matrix, leading to significantly lower values of Φ_{OH} in ice (compared to that in solution) and a discontinuity in the Φ_{OH} Arrhenius plot. Furthermore, diffusion in the bulk ice has a larger activation energy ($E_a = 50$ kJ mol^{-1}; ref 37) compared to Φ_{OH} in solution ($E_a = 19$ kJ mol^{-1}; Table 1). Therefore, Φ_{OH} in bulk ice would drop off more quickly with decreasing temperature compared to values in solution, i.e., the slope of the ice portion of the Arrhenius plot (Figure 6) would be steeper (more negative) than that of the liquid water portion. The suggestion that the photolysis of chromophores in ice occurs in a quasi-liquid layer has been made previously based on results for both nitrate[18] and 4-nitrophenol.[39] Other authors have shown that a quasi-liquid layer exists on water ice at temperatures as low as 200 K and that properties of the QLL are very sensitive to the presence of solutes.[28,29] This suggests that our reported temperature dependence for Φ_1 might be applicable to temperatures as low as 200 K.

4. Implications

4.1. NO_x Release in Arctic and Antarctic Snow. Several recent field studies have shown that photochemical reactions in surface snow result in the release of NO_x and have indicated that nitrate photolysis is an important source of this NO_x.[1−10] Our goal here is to use our measured values of Φ_1, in combination with values of Φ_2 from Dubowski and co-workers (Figure 5 of ref 19; values for ice without formate), to estimate the nitrate-derived flux of NO_x from the snowpacks in several of these studies. We consider both NO_2 formed from NO_3^- photolysis as well as NO formed as a result of nitrite formation via reaction 2. Given the much greater rate of sunlight absorption by NO_2^- and HNO_2,[40] we assume that photolysis of nitrite and nitrous acid are fast and that every NO_2^- formed is immediately converted to NO and $^{\bullet}OH$. Values of aerosol optical depth (0.37 for Neumeyer, 0.38 for Alert and Summit) and actinic flux used in our calculations are from the NCAR TUV model.[41] A wavelength-independent albedo of 0.93 for the snow surface was assumed [42] and ozone columns ranged from 306 to 309 Dobson units.[43]

The first field campaign we consider is Alert 2000, where NO_x release was measured from April 9 to May 6 in a snowpack containing the liquid equivalent of 8 μM nitrate and at a midday temperature of ∼240 K.[5] During this campaign Beine et al.[5] measured midday NO_x fluxes of $(0-5) \times 10^{12}$ molecules m^{-2} s^{-1}, while Zhou et al.[44] reported a midday HONO flux of 7×10^{12} molecules m^{-2} s^{-1} (measured on April 21). These latter authors suggest that the emitted HONO was primarily from reactions of photoproduced NO_2 in the snowpack; in this case the total equivalent NO_x flux should be $(7-12) \times 10^{12}$ molecules m^{-2} s^{-1}. On the basis of the data and approach of Simpson and co-workers,[45] but using the ice values for Φ_1 and Φ_2, we calculate that the rates of formation of gaseous NO_2 and NO in mid-April at midday (solar zenith angle (θ) = 71.5°) are 1.5×10^{12} and 0.5×10^{12} molecules m^{-2} s^{-1} from reactions 1 and 2, respectively. Assuming no loss due to reactions in the snowpack, this would result in a total flux of NO_x out of the snowpack of 2×10^{12} molecules m^{-2} s^{-1}. (Note that this is close to the calculated result of Simpson et al.,[45] 3×10^{12} molecules m^{-2} s^{-1}, which was based on only reaction 1 with an estimated quantum yield based on the temperature dependence reported by Zellner et al.[15]) Therefore, if the Beine et al.[5] flux is the more representative value, nitrate photolysis in the snowpack accounted for approximately 40% of the maximum flux of NO_x. However, if the HONO assertion of Zhou et al.[44] is correct, nitrate photolysis accounted for only a small portion (∼20%) of the maximum measured NO_x release at Alert. While there are significant uncertainties in the flux measurements,[5] as well as in our assumptions of nitrate concentrations and actinic flux in the snowpack, this comparison suggests either that chromophores other than nitrate are responsible for the bulk of NO_x release from the snow at Alert, or that there are uncharacterized thermal reactions in the snowpack that led to NO_x emissions.

We made a similar comparison for a study performed at Summit, Greenland on June 27, 2000, where the measured 1-h-average NO_x and HONO fluxes at midday (θ = 66.4°) were 6.2×10^{12} and 0.3×10^{12} molecules m^{-2} s^{-1}, respectively, and peak values were approximately two times higher.[2] Our calculated midday NO_x flux is 14×10^{12} molecules m^{-2} s^{-1}, based on a temperature of 263 K, the average nitrate content of the snow (4.4 μM liquid equivalent),[2] a snow density of 0.30 g cm^{-3} (ref 46), and a light attenuation coefficient in the snow of 0.080 cm^{-1} (ref 47). Our calculated flux is approximately two times higher than the 1-h-average measured NO_x + HONO flux, but is close to the peak values, suggesting that nitrate photolysis accounts for essentially all of the emitted NO_x and HONO in this study. It is interesting to note that our calculated value of the photolysis rate constant for nitrate ($j_{NO_3^-}$) at the snow surface under these conditions is 2.6×10^{-7} s^{-1}. This value is approximately 5 times smaller than the 2-h-average value ($\sim 14 \times 10^{-7}$ s^{-1}) measured at midday at Summit on June 7 in the near-surface snow (0−2 cm) with use of quartz tubes containing nitrate in acetonitrile with radical probe traps.[47] This comparison suggests that these field measurements of $j_{NO_3^-}$ are too high, perhaps because of errors in the radical probe calibration or because Φ_{OH} is different in acetonitrile than in water.[47]

Finally, we compare calculated and measured NO_x fluxes for two studies performed at Neumayer, Antarctic in February 1999 by Jones and co-workers. In the first study, the authors measured a NO_x flux of $\sim 2.4 \times 10^{12}$ molecules m^{-2} s^{-1} from the snowpack at approximately midday (θ = 55.3°). In comparison, we calculate a flux of 2.2×10^{12} molecules m^{-2} s^{-1} at 268 K based on the typical nitrate content of Neumayer snow (50 ng g^{-1}; ref 48), a snow density of 0.45 g/cm^3 (ref 6), and a light attenuation coefficient of 0.270 cm^{-1} in the snowpack.[48] This calculated NO_x flux is very close to the measured value and to a model value reported recently by Wolff and co-workers.[48] In the second study at Neumayer, Jones et al. measured the flux of NO_x from near the center of a $\sim 10^4$ cm^3 cube of snow held

1 m above the ground.[6] Measured fluxes of NO and NO_2 at 15:00 were 1.1×10^6 and 2.1×10^6 molecules cm^{-3}•snow s^{-1}, respectively. We calculate a NO_x flux of 6.8×10^6 molecules cm^{-3}•snow s^{-1}, using values described above, and an average nitrate value of 40 ng g^{-1} in the snowblock.[6] This calculated NO_x flux is approximately twice as high as the measured flux, suggesting that nitrate was the dominant NO_x source in the snowblock and that much of the photoformed NO_x escaped from the snowblock rather than being sampled. Thus, in contrast to the data from Alert, where nitrate photolysis accounted for only ~20−40% of the measured NO_x + HONO flux, it appears that nitrate photolysis accounts for essentially all of the measured snowpack flux of NO_x at both Neumayer and Summit. In addition to its importance as a source of NO_x, nitrate photolysis in snowpacks will also be a source of •OH, which is likely to have important effects on the chemistry of the snow and the overlying atmosphere.[11,49]

4.2. NO_x Release in Cirrus Clouds. Recent studies of the upper troposphere have indicated that photochemical models typically underestimate the $[NO_x]/[HNO_3]$ ratio.[50] Honrath and co-workers[2] have hypothesized that this might be due to the photochemical conversion of HNO_3 into NO_x on cirrus ice clouds. We have investigated the potential importance of this mechanism under typical upper tropospheric conditions modeled by Jaeglé et al.:[50] summer, ~10 km altitude (P = 0.35 atm), 35° N, 238 K, and steady-state mixing ratios of HNO_3 and NO_x of 240 and 80 pptv, respectively. On the basis of the lifetime of NO_x under these conditions (6 days),[50] the rate of loss of NO_x is 1600 molecules cm^{-3} s^{-1} (24-h average). If we (i) assume all of the HNO_3 is sorbed to ice particles, (ii) use our measured values of $\epsilon_{NO_3^-}$ (Figure 3), (iii) use extrapolated values for Φ_1 (1.7×10^{-3}) and Φ_2 (6.0×10^{-4}; ref 19) at 238 K, and (iv) use actinic flux values extrapolated from Finlayson-Pitts and Pitts,[38] we calculate that the 24-h-average rate of NO_2 production via photolysis of HNO_3 on cirrus ice particles is 110 mlc cm^{-3} s^{-1}. This rate is much slower than that needed to maintain steady state for NO_x (1600 mlc cm^{-3} s^{-1}). In contrast, we calculate that the rate of NO_x formation from the photolysis of 240 pptv HNO_3 in the gas phase is fast enough (~1400 mlc cm^{-3} s^{-1}) to approximately maintain steady state, based on a quantum yield of 1 and absorption cross sections tabulated in Finlayson-Pitts and Pitts.[38] These results suggest that photolysis of nitrate on cirrus ice particles is a minor source of NO_x that cannot resolve the underestimation of the $[NO_x]/[HNO_3]$ ratio in models. However, the large difference in the values for Φ_{OH} (and the corresponding rates of nitrate photolysis and NO_x formation) in the gas phase and on ice particles illustrates the need to accurately determine the phase of measured nitrate in field experiments to properly model NO_y chemistry in the upper troposphere.

Acknowledgment. This work was funded by the Office of Polar Programs at the National Science Foundation (OPP-9907434). Special thanks to Richard Honrath, Jack Dibb, and Paul Shepson for getting us involved in the field of ice and snow photochemistry. We also appreciate the thoughtful comments of the anonymous reviewers.

Supporting Information Available: Table S1 containing the yields of *p*-hydroxybenzoic acid (Y_{p-HBA}) resulting from the reaction of •OH with benzoic acid (BA) on ice and Table S2 containing molar absorptivities for aqueous nitrate ($\epsilon_{NO_3^-,\lambda}$) as a function of temperature and wavelength. This material is available free of charge via the Internet at http://pubs.acs.org.

References and Notes

(1) Honrath, R. E.; Peterson, M. C.; Guo, S.; Dibb, J. E.; Shepson, P. B.; Campbell, B. *Geophys. Res. Lett.* **1999**, *26*, 695.
(2) Honrath, R. E.; Lu, Y.; Peterson, M. C.; Dibb, J. E.; Arsenault, M. A.; Cullen, N. J.; Steffen, K. *Atmos. Environ.* **2002**, *36*, 2629.
(3) Dibb, J. E.; Arsenault, M. A.; Peterson, M. C.; Honrath, R. E. *Atmos. Environ.* **2002**, *36*, 2501.
(4) Ridley, B.; Walega, J.; Montzka, D.; Grahek, F.; Atlas, E.; Flocke, F.; Stroud, V.; Deary, J.; Gallant, A.; Boudries, H.; Bottenheim, J.; Anlauf, K.; Worthy, D.; Sumner, A. L.; Splawn, B.; Shepson, P. *J. Atmos. Chem.* **2000**, *36*, 1.
(5) Beine, H. J.; Honrath, R. E.; Dominé, F.; Simpson, W. R.; Fuentes, J. D. *J. Geophys. Res.-Atmos.* **2002**, *107*, 4584.
(6) Jones, A. E.; Weller, R.; Wolff, E. W.; Jacobi, H. W. *Geophys. Res. Lett.* **2000**, *27*, 345.
(7) Jones, A. E.; Weller, R.; Anderson, P. S.; Jacobi, H. W.; Wolff, E. W.; Schrems, O.; Miller, H. *Geophys. Res. Lett.* **2001**, *28*, 1499.
(8) Honrath, R. E.; Peterson, M. C.; Dziobak, M. P.; Dibb, J. E.; Arsenault, M. A.; Green, S. A. *Geophys. Res. Lett.* **2000**, *27*, 2237.
(9) Hoffman, M. R. In *Chemical Exchange Between the Atmosphere and Polar Snow*; Wolff, E. W., Bales, R. C., Eds.; Springer-Verlag: Berlin, Germany, 1996; Vol. 43; p 353.
(10) Honrath, R. E.; Guo, S.; Peterson, M. C.; Dziobak, M. P.; Dibb, J. E.; Arsenault, M. A. *J. Geophys. Res.-Atmos.* **2000**, *105*, 24183.
(11) Dominé, F.; Shepson, P. B. *Science* **2002**, *297*, 1506.
(12) Dibb, J. E.; Talbot, R. W.; Munger, J. W.; Jacob, D. J.; Fan, S. M. *J. Geophys. Res.-Atmos.* **1998**, *103*, 3475.
(13) Zepp, R. G.; Hoigné, J.; Bader, H. *Environ. Sci. Technol.* **1987**, *21*, 443.
(14) Warneck, P.; Wurzinger, C. *J. Phys. Chem.* **1988**, *92*, 6278.
(15) Zellner, R.; Exner, M.; Herrmann, H. *J. Atmos. Chem.* **1990**, *10*, 411.
(16) Mack, J.; Bolton, J. R. *J. Photochem. Photobiol. A: Chem.* **1999**, *128*, 1.
(17) Alif, A.; Boule, P. *J. Photochem. Photobiol. A: Chem.* **1991**, *59*, 357.
(18) Dubowski, Y.; Colussi, A. J.; Hoffmann, M. R. *J. Phys. Chem. A* **2001**, *105*, 4928.
(19) Dubowski, Y.; Colussi, A. J.; Boxe, C.; Hoffmann, M. R. *J. Phys. Chem. A* **2002**, *106*, 6967.
(20) Anastasio, C.; McGregor, K. G. *Atmos. Environ.* **2001**, *35*, 1079.
(21) Zhou, X. L.; Mopper, K. *Marine Chem.* **1990**, *30*, 71.
(22) Arakaki, T.; Faust, B. C. *J. Geophys. Res.-Atmos.* **1998**, *103*, 3487.
(23) Arakaki, T. Personal communication.
(24) Anastasio, C.; Faust, B. C.; Allen, J. M. *J. Geophys. Res.-Atmos.* **1994**, *99*, 8231.
(25) Berland, B. S.; Foster, K. L.; Tolbert, M. A.; George, S. M. *Geophys. Res. Lett.* **1996**, *23*, 2757.
(26) Sadtchenko, V.; Ewing, G. E. *J. Chem. Phys.* **2002**, *116*, 4686.
(27) Doppenschmidt, A.; Butt, H.-J. *Langmuir* **2000**, *16*, 6709.
(28) Cho, H.; Shepson, P. B.; Barrie, L. A.; Cowin, J. P.; Zaveri, R. *J. Phys. Chem. B* **2002**, *106*, 11226.
(29) Wei, X.; Miranda, P. B.; Shen, Y. R. *Phys. Rev. Lett.* **2001**, *86*, 1554.
(30) Adamson, A. W. *Physical Chemistry of Surfaces*, 4th ed.; John Wiley: New York, 1982.
(31) Clegg S. L.; Brimblecombe P.; Wexler A. S. *J. Phys. Chem. A* **1998**, *102*, 2137. Used web version at: mae.ucdavis.edu/wexler/aim.html.
(32) Seinfeld, J. H.; Pandis, S. N. *Atmospheric Chemistry and Physics: From Air Pollution to Climate Change*; Wiley: New York, 1998.
(33) Graedel, T. E.; Weschler, C. J. *Rev. Geophys. Space Phys.* **1981**, *19*, 505.
(34) Yang, H.; Finlayson-Pitts, B. J. *J. Phys. Chem. A* **2001**, *105*, 1890.
(35) Toom-Sauntry, D.; Barrie, L. A. *Atmos. Environ.* **2002**, *36*, 2683.
(36) Chen, W.-J.; Lo, W.-J.; Cheng, B.-M.; Lee, Y.-P. *J. Chem. Phys.* **1992**, *97*.
(37) Thibert, E.; Dominé, F. *J. Phys. Chem. B* **1998**, *102*, 4432.
(38) Finlayson-Pitts, B. J.; Pitts, J. N. *Chemistry of the Upper and Lower Atmosphere: Theory, Experiments, and Applications*; Academic Press: San Diego, CA, 2000.
(39) Dubowski, Y.; Hoffmann, M. R. *Geophys. Res. Lett.* **2000**, *27*, 3321.
(40) Arakaki, T.; Miyake, T.; Hirakawa, T.; Sakugawa, H. *Environ. Sci. Technol.* **1999**, *33*, 2561.
(41) TUV model, version 4.1, www.acd.ucar.edu/TUV/.
(42) Dickerson, R. R.; Stedman, D. H.; Delany, A. C. *J. Geophys. Res.* **1982**, *87*, 4933.
(43) TOMS data, http://toms.gsfc.nasa.gov/.
(44) Zhou, X. L.; Beine, H. J.; Honrath, R. E.; Fuentes, J. D.; Simpson, W.; Shepson, P. B.; Bottenheim, J. W. *Geophys. Res. Lett.* **2001**, *28*, 4087.
(45) Simpson, W. R.; King, M. D.; Beine, H. J.; Honrath, R. E.; Zhou, X. L. *Atmos. Environ.* **2002**, *36*, 2663.
(46) Albert, M. R.; Shultz, E. F. *Atmos. Environ.* **2002**, *36*, 2789.

(47) Qiu, R.; Green, S. A.; Honrath, R. E.; Peterson, M. C.; Lu, Y.; Dziobak, M. *Atmos. Environ.* **2002**, *36*, 2563.
(48) Wolff, E. W.; Jones, A. E.; Martin, T. J.; Grenfell, T. C. *Geophys. Res. Lett.* **2002**, *29*, 1944.
(49) Anastasio, C.; Jordan, A. Submitted to *Atmos. Environ*.
(50) Jaeglé, L.; Jacob, D. J.; Wang, Y.; Weinheimer, A. J.; Ridley, B. A.; Campos, T. L.; Sachse, G. W.; Hagen, D. E. *Geophys. Res. Lett.* **1998**, *25*, 1705.
(51) Lide, D. R., Ed. *CRC Handbook of Chemistry and Physics*, 80th ed.; CRC Press: Boca Raton FL, 1999.